Eur. Phys. J. Plus (2020) 135:677
https://doi.org/10.1140/epjp/s13360-020-00698-w

THE EUROPEAN PHYSICAL JOURNAL PLUS

Regular Article

Feasibility of using 10 MeV electron LINAC for explosives detection based on thermal neutron activation analysis: a Monte Carlo study

Mustafa Mohammad Rafiei[a], **Hossein Tavakoli-Anbaran**[b]

Faculty of Physics and Nuclear Engineering, Shahrood University of Technology, Shahrood, Iran

Received: 27 March 2020 / Accepted: 14 August 2020 / Published online: 26 August 2020

Abstract In the present paper, we used the MCNPX code for the feasibility of the design of a conceptional explosives detection system based on a neutron source generated by a 10 MeV electron linear accelerator (LINAC). In this study, an optimized e–γ–n converter (as a suitable neutron source) has been used for explosives detection based on thermal neutron activation analysis (TNAA) (a nondestructive technique for materials analysis). After optimization, total and thermal neutron fluxes of $4.78 \times 10^8 \pm 0.63\%$ (n/cm^2 mA s) and $3.95 \times 10^8 \pm 0.69\%$ (n/cm^2 mA s) could be obtained, respectively. Twelve $LaBr_3$ (3-inch) scintillator detectors have been simulated in order to calculate the response function (by the F8 tally) and to obtain a spectrum of prompt gamma of six common explosives (TNT, PETN, RDX, HMX, NG and EGDN). In these spectra, peaks of the prompt gamma of the hydrogen and nitrogen at 2.223 MeV and 10.829 MeV were observed, respectively, as the first indicator for explosives detection. The ratio of the counts under the peaks for H and N (as the second indicator for explosives detection) were also calculated. Finally, we verified the obtained results of the simulation with the theory and we showed that the results of theory and simulation have a good agreement. Therefore, the results revealed that using a 10 MeV LINAC can be a good alternative for TNAA and also for explosive detection.

1 Introduction

The activation analysis was made in 1934 by Irene Joliot Curie and Frederic Joliot who used alpha particles for bombarded aluminum, boron and magnesium [1–3]. In 1936, the activation analysis was done for element analysis by Hevesy and Levi who bombarded dysprosium and europium by neutrons [1, 3]. Two years later, in 1938, Seaborg and Livingood bombarded the iron sample with deuterons for the determination of the gallium [3]. Therefore, it can be concluded that the selection of the source for activation analysis is important. One of the practical sources for activation analysis is neutron. For this aim, several neutron sources exist today, including nuclear reactors, accelerators, and isotopic sources. As mentioned above, the neutron activation analysis was introduced for element analysis many years ago since it is a nondestructive analysis. Therefore, in this work, we used thermal neutrons for activation

[a] e-mail: mustafa.m.rafiei@gmail.com (corresponding author)
[b] e-mail: tavakoli.anbaran@gmail.com

of samples. In this method, the nucleus of the target is bombarded by thermal neutrons. When a thermal neutron capture by a nucleus is done, one or more prompt characteristic gamma released rapidly of the compound nucleus [4–6] and this is called as the thermal neutron activation analysis (TNAA). We could detect these prompt gammas by suitable gamma detectors (such as solid-state detectors [7–9] and scintillator detectors [10–12]) and this is also called as prompt gamma neutron activation analysis (PGNAA). One can find good literature for recent developments and applications of PGNAA in Ref. [13]. However, the sensitivity of PGNAA depends on the thermal neutron flux. Therefore, the nuclear reactors are more commonly used because of their high considerable neutron flux. But nuclear reactors are expensive and cannot be used everywhere. Therefore, we need another neutron source that has acceptable neutron flux and is cheaper and portable. One of the neutron sources having previous conditions is the neutron source that has been generated by an electron linear accelerator (LINAC) [14]. Recently, many works have been done on the development of neutron sources generated by electron LINAC [15–18]. These sources could be used to detect explosives based on the thermal neutron activation, for example, one can find the other works [19, 20]. However, in this study, we used a 10 MeV electron LINAC for investigation of feasibility of explosives detection (TNT, PETN, RDX, HMX, NG and EGDN) based on TNAA. For this aim, we optimized an *e*–γ–*n* converter to reach suitable high thermal neutron flux using MCNPX 2.7 Monte Carlo code [21]. It should be mentioned that there are other portable neutron sources also, which have been used to detect explosives such as neutron generators (D–D and D–T) [22–24], californium-252 [24–27] and americium–beryllium [24, 28, 29]. However, for optimization of the *e*–γ–*n* converter, we studied ten suitable materials to use as neutron collimator/reflector. Finally, the BeD_2 was chosen as the best material. Also, the optimized length of the collimator was chosen as 60 cm by Monte Carlo simulation. Because of an intense bremsstrahlung photons flux that emitted from the aperture of the *e*–γ–*n* converter along with neutrons we chose 30 cm Lead by Monte Carlo simulation to reduce intense photons flux. After all of simulation and optimization of *e*–γ–*n* converter, we could reach to $4.78 \times 10^8 \pm 0.63\%$ (n/cm^2 mA s) total neutron flux and $3.95 \times 10^8 \pm 0.69\%$ (n/cm^2 mA s) thermal neutron flux. The neutron flux can collide with explosives and activate the elements of them (H, C, N, O) through neutron capture reaction. Therefore, we need a suitable gamma detector to record the prompt gamma rays. For this aim, twelve $LaBr_3$ (3-inch) were simulated, because the $LaBr_3$ detector has a better resolution than the NaI detector and also has greater density and faster decay time [30]. The $LaBr_3$ also is cheaper than HPGe detector and there is no need to use liquid nitrogen for cooling [30]. Note that liquid nitrogen of the HPGe detector can trouble the spectrum of prompt gamma rays of nitrogen emitted from explosives. After collecting the prompt gamma rays spectrum, we observed the peaks of prompt gamma of H and N clearly (at 2.223 MeV and 10.829 MeV, respectively). Finally, we could calculate the ratio of the counts under the peaks of H and N along with a good agreement between the results of simulation and theory. This agreement showed that we can use a 10 MeV LINAC for TNAA and explosive detection, as well. In addition, note that the dependency of converter dimensions on linear accelerator dimensions is important, because different accelerators have different dimensions. Certainly, in the future studies, the converter designed in this paper should be considered in terms of photon and neutron dosimetry. Since neutrons and photons can escape this converter and as a final point, it should be noted that the converter designed in this work can also be used in boron neutron capture therapy [31], nuclear waste transmutation [32], and isotope production [33].

2 Materials and method

In the present paper, the MCNPX 2.7 Monte Carlo code has been used for all simulations. The MCNPX is a comprehensive 3-dimentional Monte Carlo code that it can simulate many particles (such as electron, photon and neutron, etc.) and reactions (such as atomic and nuclear reaction) [21]. For simulation of the electron, photon and neutron el03, mcplib04 and ENDF/B-VII.0 cross section library have been used, respectively (el03, mcplib04, and ENDF/B-VII.0 are the name of the cross section library of the electron, photon, and neutron in the MCNP code, respectively). However, we used a 10 MeV LINAC as an electron source with the properties mentioned in Ref. [34] (the accelerating tube length of a 10 MeV electron LINAC can be 1.6 m [35] or 1.7 m [36]) and in order to define the electron source card in the MCNPX, we used from Ref. [14]. Also, $LaBr_3$ (3-inch) scintillator detector has been used to obtain the prompt gamma spectrum emitted from the explosives [37].

3 The *e–γ–n* converter optimization

In this work, we used a 10 MeV LINAC for generation of a good neutron source. For this aim, we used a good reference that designed an *e–γ–n* converter based on 10 MeV LINAC [34]. But in our work, in order to use in TNAA, we studied again the previous design for suitable optimization. Note that we only studied the length and the material type of the collimator of the previous *e–γ–n* converter and did not change the other parts of the *e–γ–n* converter. After all optimizations and changes mentioned (in detail) in the following, the new optimized cylindrical *e–γ–n* converter based on the 10 MeV electron LINAC is shown in Fig. 1. Briefly, the method of generation of a neutron source from an electron accelerator is that the energetic electrons collide with a high atomic number target (such as tungsten) and lead to a relatively intense flux of bremsstrahlung photons and then these photons collide with a photonuclear target (such as beryllium or heavy water) and lead to a significant neutrons flux. For more information on the *e–γ–n* converter design method, one can see Ref. [14].

Ten materials (Be, BeD_2, BeO, D_2O, graphite, Al_2O_3, H_2O, PE, ZrH_2, and Pb) have been studied for the determination of the best collimator and reflector by MCNPX 2.7 Monte Carlo Code (along with ENDF/B-VII.0 neutron cross section library) whose properties are shown in Table 1. Also, the length of the collimator (the distance between the aperture and D_2O target as a gamma-neutron converter) has been investigated. Four parameters have been studied for determination of the best material. These parameters include $C_1 = \emptyset_{th}^2/\emptyset_{total}\left(\mathrm{n/cm^2\ mA\ s}\right)$, $C_2 = \emptyset_{th}/\emptyset_{epi}$, $C_3 = \emptyset_{th}/\emptyset_{fast}$ and $C_4 = \emptyset_{th}/\emptyset_{(epi+fast)}$ where $\emptyset_{th}$, $\emptyset_{epi}$, $\emptyset_{fast}$ and $\emptyset_{total}$ are thermal ($<10^{-6}$ MeV), epithermal (10^{-6}–10^{-2} MeV), fast ($>10^{-2}$ up to 20 MeV) and total neutron flux, respectively [38] (Fig. 2). The parameter C_1 is called the thermalization efficiency. This parameter can be used to select the point which has maximize the ratio of the thermal neutron flux to the total neutron flux and has the highest possible value of the thermal neutron flux [38].

For more confidence in the optimization of the distance between D_2O to aperture, the thermal neutron flux has been investigated, as shown in Fig. 3. It should be noted that the aperture diameter is considered 40 cm, because we intend to optimize the *e–γ–n* converter based on practical cases. One of the practical cases is detecting possible explosives in the luggage of airport passengers by TNAA. Note that the common approved size of the luggage based on some popular airlines such as United Airlines, American Airlines and Lufthansa Airlines is (56 cm × 35 cm × 22 cm) [40], (56 cm × 36 cm × 23 cm) [41] and (55 cm × 40 cm × 23 cm) [42], respectively (in format: length × width × height). Given that the increase

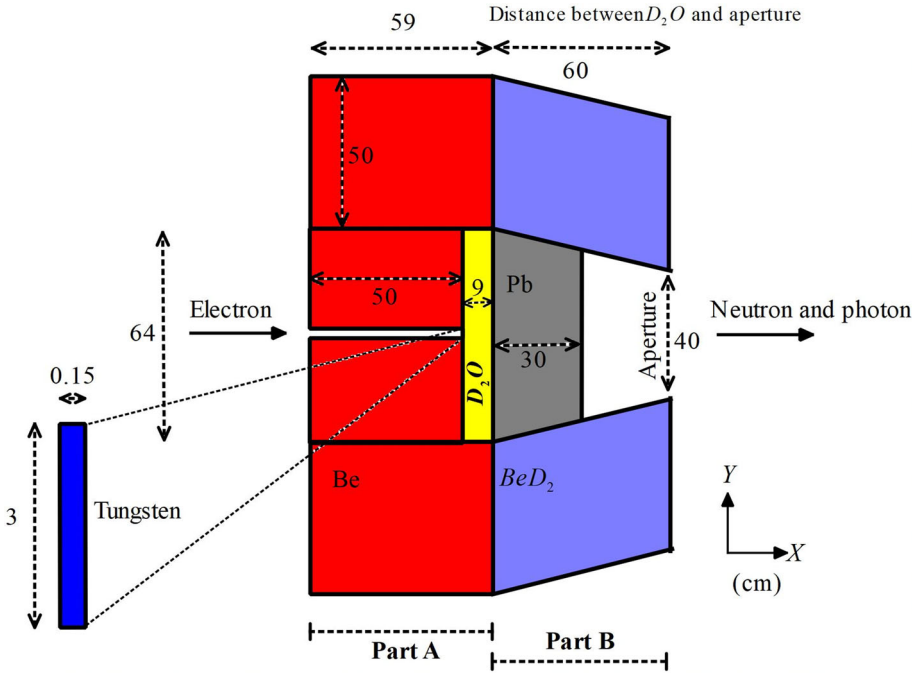

Fig. 1 Scheme of optimized the cylindrical *e*–γ–*n* converter based on 10 MeV electron LINAC, part A from Ref. [34] and part B from the present work (the 2D view) (all dimensions are in cm)

Table 1 The properties of materials utilized in the *e*–γ–*n* converter optimization [16, 38, 39]

Materials	Density (g/cm^3)	Atomic fraction
Be	1.848	Be (1)
BeD_2	0.765	Be (0.3333), D (0.6667)
BeO	3.01	Be (0.5), O (0.5)
D_2O	1.105340	D (0.6667), O (0.3333)
Graphite	1.7	C (1)
Al_2O_3	3.97	Al (0.4), O (0.6)
H_2O	0.998207	H (0.6667), O (0.3333)
PE	0.93	C (0.333338), H (0.666662)
ZrH_2	5.61	Zr (0.3333), H (0.6667)
Pb	11.35	Pb (1)

in thermal neutron flux is desirable in this work, see Figs. 2 and 3, the BeD_2 has been chosen as the best material (because for example, the BeD_2 relative to Be and graphite can increase the thermal neutron flux up to 14% and 113%, respectively, that these percentages are based on the relative difference relationship) for use as a collimator/reflector and also the optimized length of the collimator (distance between D_2O and aperture) has been chosen as 60 cm.

As mentioned above, an intense bremsstrahlung photon flux along with the neutron flux is emitted from the aperture of the converter. We tried to reduce the intensity of these photons as much as possible, because these bremsstrahlung photons can be recorded in the spectrum of the gamma detector acting as a background signal overlapping to the prompt gamma spectrum

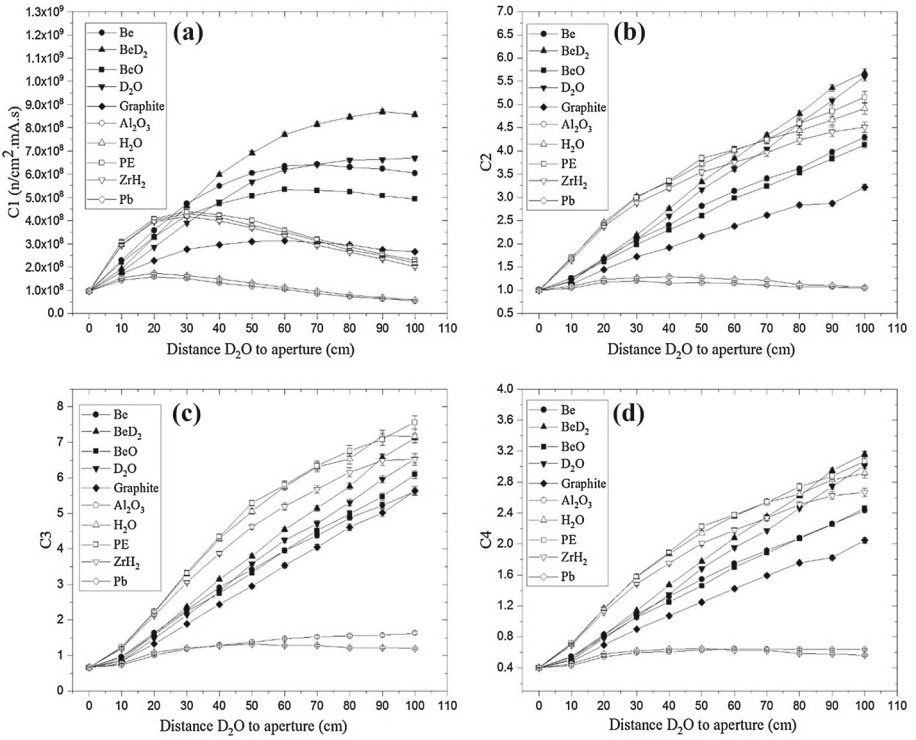

Fig. 2 The parameter **a** C_1, **b** C_2, **c** C_3 and **d** C_4 as a function of distance between D_2O and aperture

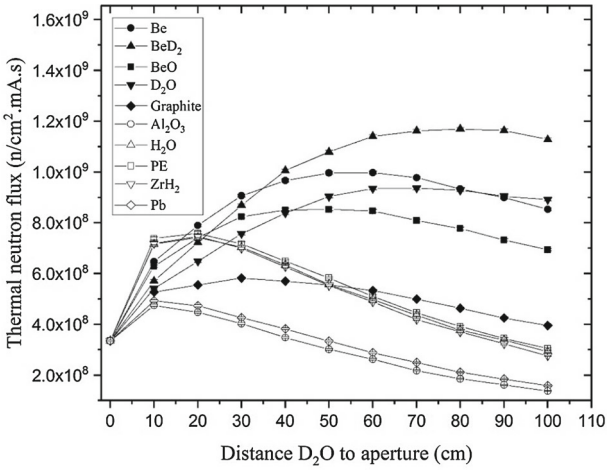

Fig. 3 Thermal neutron flux as a function of distance between D_2O and aperture

emitted from the explosive elements. Therefore, we used lead to reduce the bremsstrahlung photon flux. In fact, we placed the lead right after heavy water and to find the optimum thickness of lead, we used the Monte Carlo simulation for which the results are shown in Fig. 4. See Fig. 4, the optimum thickness of lead is 30 cm. Note that lead leads to a decrease

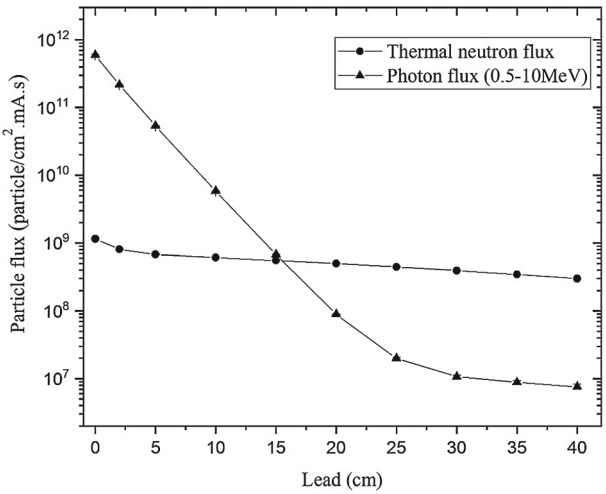

Fig. 4 Photon flux (in the energy range of 0.5–10 MeV) and thermal neutron flux as a function of the thickness of lead

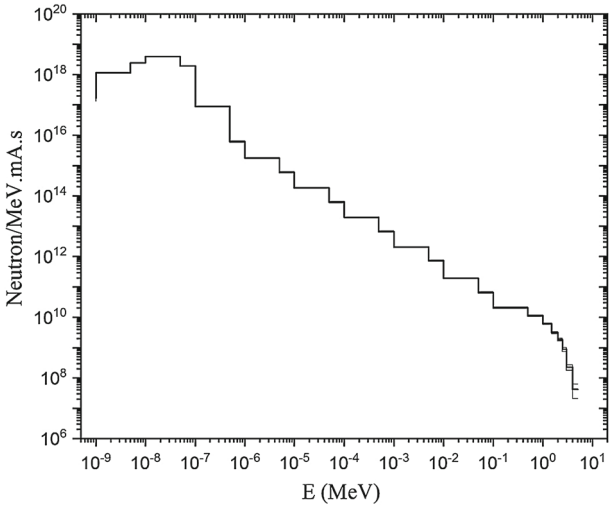

Fig. 5 Neutron energy spectrum according to the optimized *e*–γ–*n* converter (Fig. 1)

in thermal neutron flux, as well, that it is not significant as shown in Fig. 4. But the thickness of the 30 cm lead is capable of reducing the photon flux (in the energy range of 0.5-10 MeV) by approximately 10^5 times which is very significant (Table 1).

The emitted neutron spectrum from the optimized *e*–γ–*n* converter is shown in Fig. 5 that the total neutron flux and thermal neutron flux are $4.78 \times 10^8 \pm 0.63\%$ (n/cm^2 mA s), $3.95 \times 10^8 \pm 0.69\%$ (n/cm^2 mA s), respectively. Now, we can use these neutrons as a desirable neutron source for explosive detection based on TNAA. The angular distribution of neutron and photon beams emitted from the aperture of the converter is shown in Figs. 6 and 7 (as a contour plot), respectively.

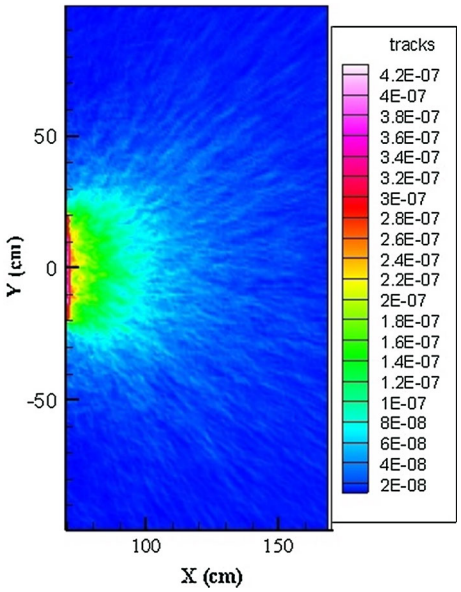

Fig. 6 Neutron tracks (per electron) have been shown for the right side of the aperture in Fig. 1 and note that the origin of the horizontal axis (X-axis) has been placed on the tungsten target

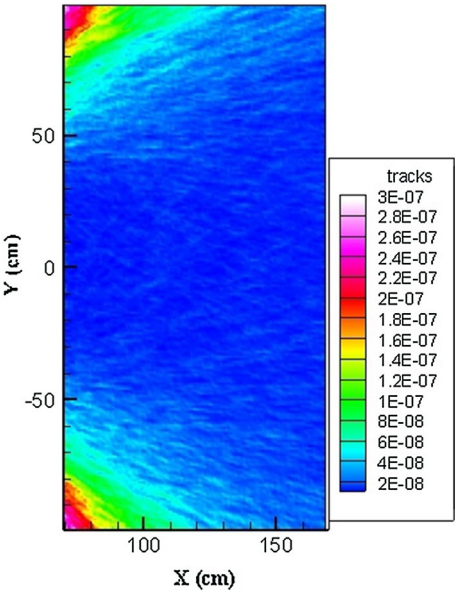

Fig. 7 Photon tracks (per electron) have been shown for the right side of the aperture in Fig. 1 and note that the origin of the horizontal axis (X-axis) has been placed on the tungsten target

4 Results and discussion

4.1 Simulation of TNAA

As shown in the previous section, we obtained a suitable neutron spectrum with acceptable flux for use in explosives detection based on TNAA. To perform the Monte Carlo simulation, we chose six commonly cylindrical sample explosives (TNT, PETN, RDX, HMX, NG, and

Table 2 The properties of six commonly explosives [39]

Materials	Chemical formula	Density (g/cm^3)	Atomic fraction
TNT	C6H2(NO2)3CH3	1.65	H (0.238095), C (0.333333), N (0.142857), O (0.285714)
PETN	C5H8N4O12	1.77	H (0.275862), C (0.172414), N (0.137931), O (0.413793)
RDX	C3H6N6O6	1.82	H (0.285714), C (0.142857), N (0.285714), O (0.285714)
HMX	C4H8N8O8	1.89	H (0.285714), C (0.142857), N (0.285714), O (0.285714)
NG	C3H5N3O9	1.60	H (0.250000), C (0.150000), N (0.150000), O (0.450000)
EGDN	C2H4N2O6	1.49	H (0.285714), C (0.142857), N (0.142857), O (0.428571)

EGDN) with a mass of 1 kg and a radius of 5 cm for which the properties are listed in Table 2. The commonly explosives are made up of four elements: hydrogen, nitrogen, carbon, and oxygen (Table 2). After the thermal neutron capture reaction, hydrogen, nitrogen, carbon, and oxygen elements emitted one, eighteen, four, and three prompt gamma rays, respectively [43] and we observed all of prompt gamma rays of H, N, C, and O by F1 tally (current integrated over a surface [21]) using ENDF/B-VII.0 neutron cross section library.

But, in this study, the F1 tally is not desired, because we are looking for the response function of the gamma ray detector to analyze the spectrum of the prompt gamma rays emitted by the explosives, and therefore, we used F8 tally (energy distribution of pulses created in a detector by radiation [21]). In this work, we used twelve $LaBr_3$ (3-inch), because no variance reduction cards can be used to reduce statistical errors when using the F8 tally along with neutron source in MCNPX code [21]. Therefore, we tried to reduce the statistical error by increasing the number of detectors. The setup of twelve $LaBr_3$ gamma detectors is shown in Fig. 8. Note that the distance of detectors from the center of the cylindrical explosives is 21 cm, because the radius of aperture of the e–γ–n converter is 20 cm. The $LaBr_3$ detector is an interesting gamma-ray detector for TNAA because of its faster decay time, higher density and better resolution than the NaI detector and also it is cheaper than the HPGe detector and there is no need to use liquid nitrogen for cooling [30]. For the simulation of the gamma detectors, we used the F8 tally along with FT (special treatments for tallies [21]) and GEB (Gaussian energy broadening [21]) cards in order to apply full-width of half maximum (FWHM) on all of the $LaBr_3$ detectors. The MCNPX code uses the following equation as the FWHM (in MeV) function [21].

$$\mathrm{FWHM} = A + B\sqrt{E + CE^2} \tag{1}$$

where E is energy of photon in MeV, A, B and C are coefficients in MeV, $(\mathrm{MeV})^{1/2}$, and $(\mathrm{MeV})^{-1}$, respectively. We found the coefficients A, B and C through fitting data of Ref. [37] as -0.007836, 0.03858 and 0.001, respectively.

In Fig. 8, the emitted neutron and photon beams from the e–γ–n converter are assumed in the direction of + Z-axis and the $LaBr_3$ detectors were placed at a 90-degree angle relative to the + Z-axis, because in this direction there is a minimum of scattered photons. This is in agreement to the Klein–Nishina formula for Compton scattering [30]. In fact, in this study, we assumed that the neutron and photon beams emitted from the e–γ–n converter are

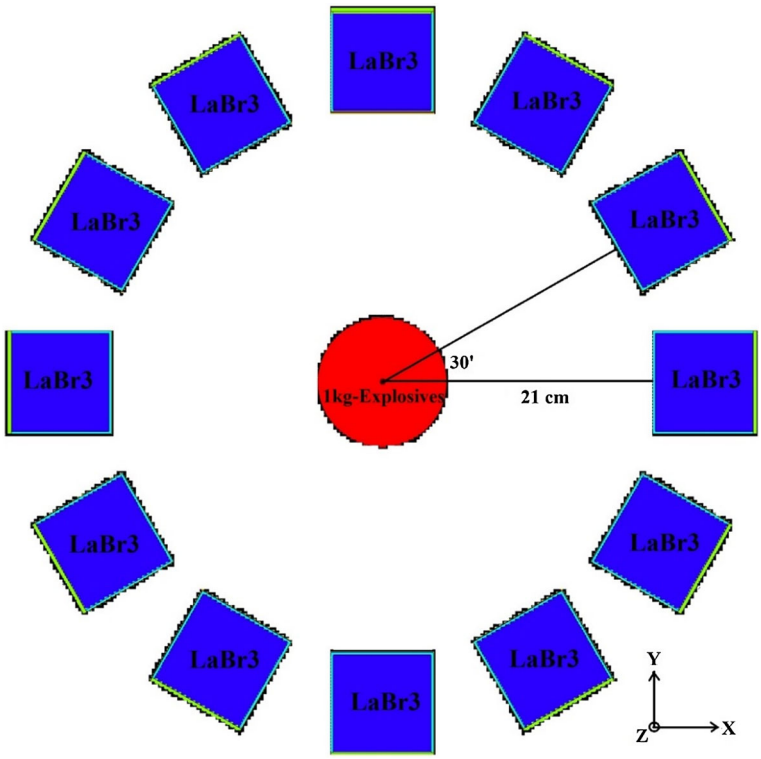

Fig. 8 Setup of twelve $LaBr_3$ (3-inch) gamma detectors around 1 kg cylindrical explosives (the radius of all cylindrical explosives samples is 5 cm) (the 2D view)

cylindrical and parallel to the Z-axis. The assumption that the neutron beams are parallel can be acceptable and reasonable for two reasons, the first, increasing or decreasing the colliding neutrons with the explosive only leads to a change in the number of prompt gamma rays and no change in the overall shape of the prompt gamma spectrum (the reader can pay attention to the described equations in the next section). In fact, using the actual neutron angular distribution only reduces the number of prompt gamma rays (because the overall shape of the prompt gamma spectrum depends on the neutron energy spectrum or in the other words depends on the cross section of neutron capture reaction and it does not depend on the neutron flux) that can be solved by increasing the irradiation time and the second, using the assumption of parallel beams can very effectively help reduce the statistical error of the F8 tally and it enables us to do a good validation in the next section. In order to reduce statistical error, the diameter of the cylindrical beams of neutron and photon had been assumed 10 cm, because the diameter of 1 kg of the introduced cylindrical explosives is 10 cm and therefore all of the neutron and photon collide with cylindrical explosives. After doing the above, we perform Monte Carlo simulation for finding spectrum of prompt gamma rays of six explosives (TNT, PETN, RDX, HMX, NG, and EGDN) with mass 1 kg that in these spectrums the peaks of prompt gamma ray of H (2.223 MeV), N (10.829 MeV) and single escape (1.712 MeV & 10.318 MeV) clearly observed. For example, the spectrum of prompt gamma ray of TNT is shown in Fig. 9. Unfortunately, because of the low thermal neutron capture cross section of carbon and oxygen relative to hydrogen and nitrogen, their prompt gamma rays were not

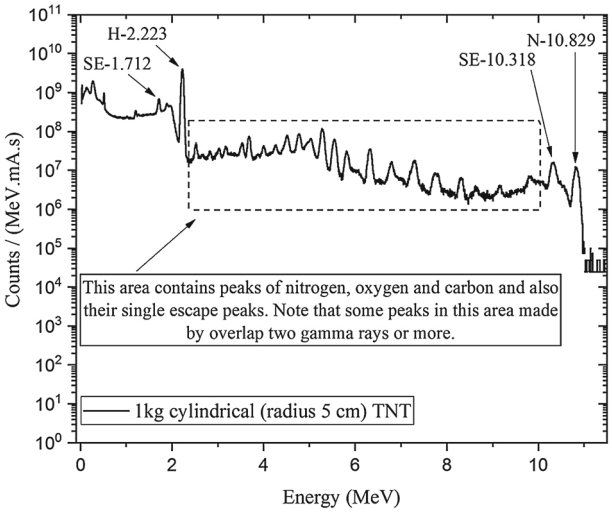

Fig. 9 The spectrum of prompt gamma (collected by twelve $LaBr_3$ gamma detectors) of 1 kg cylindrical TNT by MCNPX

found in the gamma spectrum [43]. Note that the simultaneous observation of hydrogen and nitrogen prompt gamma peaks can be an indicator for detecting explosives.

It is good to mention that neutrons also activate lead as they pass through the shield (Fig. 4). Given that we assumed emitted photon beams from converter are parallel (described above) and also given the Compton angular distribution (described above), therefore, the probability of observation of prompt gamma of lead decreases in Fig. 9. If prompt gamma rays of lead are observed in the spectrum, but fortunately they cannot overlap with the peaks of H (2.223 MeV) and N (10.829 MeV), because the energy of the prompt gamma rays of lead are 6.737 MeV and 7.367 MeV [43]. Of course, in an experimental scenario, we may observe more prompt gamma peaks in Fig. 9 such as prompt gamma of aluminum, lanthanum and bromine. But according to Ref. [43] the prompt gamma ray energies of these materials are far from the peaks of H (2.223 MeV) and N (10.829 MeV). Even if the energy of their prompt gamma rays is a little close to the peaks of H and N but their neutron capture cross sections are much smaller [43]. Therefore, they cannot cause a significant problem in the peaks of H (2.223 MeV) and N (10.829 MeV). Of course, we can reduce the number of neutrons that may reach to detectors by adding collimator as well as appropriate shield. Another point that may lead to gamma spectrum disorder in experimental conditions, is the pile-up [30, 44]. The pile-up occurs when two or more gamma rays detected almost simultaneously in the detector. But this effect can be reduced significantly by specific electronic circuits and also algorithms [44, 45]. In the following, we studied and estimated some materials (including lead, cadmium, and boron) for the shielding of the $LaBr_3$ detector. For this aim, we used a simple but practical geometry for the study of photon and neutron shielding as shown in Fig. 10.

For the investigation of the shielding of neutron and photon, a cylindrical shield (Fig. 10) has been exposed to radiation by the obtained neutron and photon beam from the converter (Fig. 1). Given that 83% of the neutrons emitted from the converter are thermal neutrons, the choice of boron and cadmium as a neutron shield can be good, because these two materials have a high thermal neutron absorption cross section [43]. On the other hand, boron has only

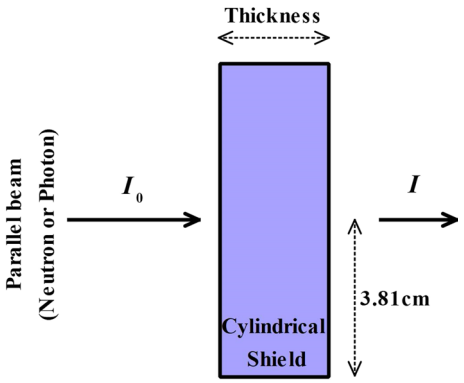

Fig. 10 The geometry used for the investigation of the shield (the radius of the cylindrical shield is related to the size of the detector window)

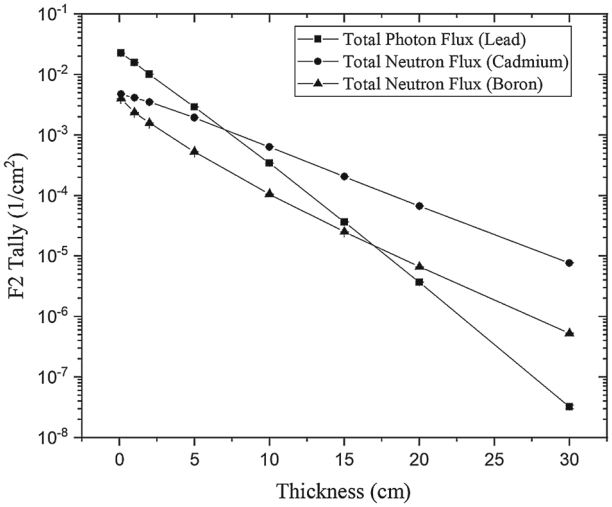

Fig. 11 Particle flux after passing through the shield relative to the thickness of the shield

one prompt gamma in 0.480 MeV energy and the maximum energy of prompt gamma of cadmium is 1.399 MeV that these energies are significantly different from the prompt gamma of hydrogen [43]. In Fig. 11, you can see the simulation results by F2 tally (flux averaged over a surface) of the MCNPX code for the three materials, lead (as the photon shield), cadmium, and boron. As shown in Fig. 11, boron has better results than cadmium, because boron, in addition to having a high absorption cross section for thermal neutrons, has a lower atomic number than cadmium, therefore it can also act as a moderator.

4.2 Validation of TNAA

As mentioned above, the simultaneous presence of prompt gamma peaks of hydrogen and nitrogen can be used as a marker for detecting explosives, but it seems not enough for the accurate detection. Therefore, we must define another indicator which can be the ratio of the counts under the prompt gamma peaks of H (2.223 MeV) and N (10.829 MeV). We can calculate and compare the ratio for theory and the simulation. However, to calculate the ratio by simulation, we simply fit a Gaussian function onto the prompt gamma peaks of H and N

(in Fig. 9). One can find good explanations on how to calculate counts under prompt gamma peaks based on gamma spectrum in Ref. [3]. To calculate the ratio by theory, we can begin from the following equation [3].

$$R_i\,(\text{reactions}/s) = I\left(\frac{\text{n}}{\text{m}^2\ \text{s}}\right) \times N_i\left(\frac{\text{nuclei}}{\text{m}^3}\right) \times a\left(\text{m}^2\right) \times t\,(\text{m}) \times \sigma_i\left(\text{m}^2\right) \tag{2}$$

where R_i is the number of reactions per second for the ith prompt gamma, I is the neutron flux, N is the number of target ith nuclide per volume, a is the area of target, t is the thickness of the target and σ_i is the microscopic neutron cross section of ith prompt gamma. To reach the counts under prompt gamma peaks, it is enough that three parameters $\in_i$, Ω and f_i multiply by R_i. Therefore, we can write the counts under peak of ith prompt gamma (C_i in counts/s) as follows.

$$C_i = I \times N_i \times a \times t \times \sigma_i \times \in_i \times \Omega \times f_i \tag{3}$$

where $\in_i$, Ω and f_i are the efficiency of ith prompt gamma peak (we can calculate it based on Fig. 8 by MCNPX, assuming the gamma rays are emitted exactly from the center of the circle with a 21 cm radius), the solid angle of detector (geometrical solid angle divided by 4π) and the factor of attenuation ith prompt gamma, respectively. Assuming all prompt gamma emit from the center of the cylindrical explosives, we can write the f_i as follows.

$$f_i = \exp\left[-\left(\frac{\mu_i}{\rho}\right)(\rho r)\right] \tag{4}$$

where μ_i [46], ρ and r are total linear attenuation coefficient of ith prompt gamma in cm^{-1}, the density of explosives in g/cm^3 and the radius of cylindrical explosives in cm, respectively. Of course, we can write N_i as follows.

$$N_i = \frac{\rho N_A A_i}{M} \tag{5}$$

where N_A, A_i and M are Avogadro number, the number of ith element and the molecular weight (in g/mol) of explosives, respectively. Finally, as mention above, we can write the ratio of the counts under prompt gamma peaks of H and N as follows.

$$\frac{C_{(\text{H}-2.223)}}{C_{(\text{N}-10.829)}} = \frac{\sigma_\text{H} \in_\text{H} f_\text{H} A_\text{H}}{\sigma_\text{N} \in_\text{N} f_\text{N} A_\text{N}} \tag{6}$$

The parameters of $\sigma_\text{H}/\sigma_\text{N}$, $\in_\text{H} / \in_\text{N}$, f_H/f_N and A_H/A_N are in Table 3 for the six explosives and also ratio of C_H/C_N both for theory and simulation and relative difference between them are shown in Table 3. See Table 3, the results of theory and simulation of ratio of the counts under prompt gamma peaks have a good agreement. There is a slight relative difference, which can be due to the assumptions we have made for theoretical calculations. According to Eq. 6, it is very good to mention that the overall shape of the prompt gamma energy spectrum is dependents on four parameters (σ, $\in$, f and A) and it does not depend on neutron flux. In fact, according to Eqs. 2 and 3, increasing or decreasing the neutron flux will only increase or decrease the number of prompt gamma rays.

For the approximate detection time, we can mention Ref. [26]. In Ref. [26], the researchers used a Cf-252 with 5.4×10^7 (neutron/s) as neutron source along with ten BGO detectors for the detection of 1.2 kg HMX in one minute. Also, please pay attention to Ref. [47], the researchers report 9 and 12 MeV electron LINAC with average current of 800 and 1000 μA, respectively. Assuming an average current of 800 μA, the thermal neutron flux reach to 3.16×10^8 (n/cm^2 s) in our work. Therefore, according to Refs. [26, 47], the explosives can be detected at a reasonable time.

Table 3 The ratio of C_H/C_N both for theory and simulation

Explosives	$\frac{\sigma_{(H-2.223)}}{\sigma_{(N-10.829)}}$ [43]	$\frac{\in_{(H-2.223)}}{\in_{(N-10.829)}}$	$\frac{f_{(H-2.223)}}{f_{(N-10.829)}}$	$\frac{A_H}{A_N}$	$\frac{C_{(H-2.223)}}{C_{(N-10.829)}}$ Theory (B)	$\frac{C_{(H-2.223)}}{C_{(N-10.829)}}$ Simulation (A)	Relative difference % $\frac{A-B}{B} \times 100$
TNT	31.0841	3.5808	0.82737	1.667	153.52	159.84 ± 1.8	4.1
PETN			0.81699	2	181.87	191.74 ± 2.2	5.4
RDX			0.81137	1	90.31	94.33 ± 0.8	4.5
HMX			0.80488	1	89.59	92.81 ± 0.8	3.6
NG			0.83387	1.667	154.72	162.26 ± 1.9	4.9
EGDN			0.84359	2	187.79	193.57 ± 2.3	3.1

5 Conclusion

In this paper, we investigated the feasibility of using a 10 MeV electron accelerator to detect explosives (TNT, PETN, RDX, HMX, NG, and EGDN) based on thermal neutron activation. To generate a suitable neutron source for detecting explosives, we designed and optimized an *e*–γ–*n* converter. Finally, we obtained $4.78 \times 10^8 \pm 0.63\%$ (n/cm^2 mA s) total neutron flux and $3.95 \times 10^8 \pm 0.69\%$ (n/cm^2 mA s) thermal neutron flux from the optimized *e*–γ–*n* converter. As seen above, a considerably good neutron source with a high and suitable thermal neutron flux was achieved. Twelve $LaBr_3$ (3-inch) scintillator detectors were used for detection of explosives based on TNAA. The prompt gamma of H (2.233 MeV) and N (10.829 MeV) were observed in the gamma spectrum clearly which could be an indicator for detecting explosives. Another indicator is the ratio of the counts under the peaks corresponding to H and N which was verified with theory in this work. It should be noted that this conceptual design for explosives detection must be evaluated for radiation shielding, as done in Ref. [48]. Finally, it can be concluded that using a 10 MeV electron LINAC can be a good option for explosives detection and TNAA, if used with the appropriate gamma detectors.

References

1. Z.B. Alfassi, *Activation Analysis,*, vol. I (CRC Press Inc, Florida, 1990)
2. Z.B. Alfassi, *Activation Analysis,*, vol. II (CRC Press Inc, Florida, 1990)
3. N. Tsoulfanidis, S. Landsberger, *Measurement and Detection of Radiation*, 4th edn. (CRC Press, New York, 2015)
4. G.L. Molnar, *Handbook of Prompt Gamma Activation Analysis with Neutron Beams* (Kluwer Academic Publishers, Boston, 2004)
5. J.N. Beck, C.M. Lamberty, Thermal neutron activation analysis an important analytical tool. Appl. Spectrosc. Rev. **37**(1), 19–55 (2002)
6. L. Hamidatou, H. Slamene, T. Akhal, B. Zouranen, Concepts, Instrumentation and Techniques of Neutron Activation Analysis (Chapter 6), in Imaging and Radioanalytical Techniques in Interdisciplinary Research, IntechOpen (2013), pp. 141–178
7. O. Sierra, et al., Characterization of HPGe gamma spectrometric detectors systems for Instrumental Neutron Activation Analysis (INAA) at the Colombian Geological Survey, in AIP Conference Proceedings (2016)
8. K. Babaeian, F. Rahmani, Y. Kasesaz, Conceptual design of prompt gamma neutron activation analysis facility at Tehran Research Reactor for BNCT application. Nucl. Instrum. Methods Phys. Res. Sect. A **935**, 185–190 (2019)

9. C. Cheng et al., Efficiency calibration of HPGe detector in a PGNAA system for the measurement of aqueous samples. Appl. Radiat. Isot. **145**, 1–6 (2019)
10. B. Ozden, C. Brennan, S. Landsberger, Environmental assessment of red mud by determining natural. Environ. Earth Sci. **78**(4), 100 (2019)
11. P. Sibczyński et al., Monte Carlo N-Particle simulations of an underwater chemical threats detection system using neutron activation analysis. J. Instrum. **14**, P09001 (2019)
12. A.A. Naqvi et al., Detection of sulfur in soil samples using 2.5 MeV neutron activation. J. Radioanal. Nucl. Chem. **321**(1), 355–360 (2019)
13. R.M. Lindstrom, Z. Révay, Prompt gamma neutron activation analysis (PGAA): recent developments and applications. J. Radioanal. Nucl. Chem. **314**(2), 843–858 (2017)
14. M.M. Rafiei, H. Tavakoli-Anbaran, Feasibility of using heavy water in order to design of a photoneutron source based on 5 MeV electron linear accelerator. J. Instrum. **13**, P05008 (2018)
15. X. Li et al., Performance of an electron linear accelerator for the first photoneutron source in China. Nucl. Sci. Tech **30**(14), 20 (2019)
16. M. Zolfaghari, S.F. Masoudi, F. Rahmani, Optimization of Linac-based neutron source for thermal neutron activation analysis. J. Radioanal. Nucl. Chem. **317**(3), 1477–1483 (2018)
17. A. Sari, F. Carrel, F. Lainé, Characterization and optimization of the photoneutron flux emitted by a 6- or 9-MeV electron accelerator for neutron interrogation measurements. IEEE Trans. Nucl. Sci. **65**(9), 2018 (2018)
18. B. Askri, Optimization of a photoneutron source based on 10 MeV electron beam using Geant4 Monte Carlo code. Nucl. Instrum. Methods Phys. Res. Sect. B **360**, 1–8 (2015)
19. Y. Yang et al., Explosives detection using photoneutrons produced by X-rays. Nucl. Instrum. Methods Phys. Res. A **579**, 400–403 (2007)
20. Y. Yang et al., Fusion of X-ray imaging and photoneutron induced gamma analysis for contrabands detection. IEEE Trans. Nucl. Sci. **60**, 110 (2013)
21. D.B. Pelowitz, MCNPX User's Manual Report LA-CP-11-00438, Los Alamos National Laboratory, 2011
22. M.C. Han et al., Experiment and MCNP simulation of a portable tagged neutron inspection system for detection of explosives in a concrete wall. Nucl. Instrum. Methods Phys. Res. Sect. A **929**, 156–161 (2019)
23. S. Bishnoi et al., Modeling of tagged neutron method for explosive detection using GEANT4. Nucl. Instrum. Methods Phys. Res. Sect. A **923**, 26–33 (2019)
24. Z.D. Whetstone, K.J. Kearfott, A review of conventional explosives detection using active neutron interrogation. J. Radioanal. Nucl. Chem. **301**(3), 629–639 (2014)
25. R.C. Martin, J.B. Knauer, P.A. Balo, Production, distribution and applications of californium-252 neutron sources. Appl. Radiat. Isot. **53**(4–5), 785–792 (2000)
26. C. Chung et al., Feasibility study of explosive detection for airport security using a neutron source. Appl. Radiat. Isot. **44**(12), 1425–1431 (1993)
27. M.N. Nasrabadi et al., Development of a technique using MCNPX code for determination of nitrogen content of explosive materials using prompt gamma neutron activation analysis method. Nucl. Instrum. Methods Phys. Res. Sect. A **659**(1), 378–382 (2011)
28. L.E. Cevallos-Robalino et al., Analysis by Monte Carlo of thermal neutron flux from a 241 Am/9Be source for a system of trace analysis in materials. Appl. Radiat. Isot. **151**, 19–24 (2019)
29. P.L. Hernández-Adame et al., Design of an explosive detection system using Monte Carlo method. Appl. Radiat. Isot. **117**, 27–31 (2016)
30. G.F. Knoll, *Radiation Detection and Measurement*, 4th edn. (Wiley, New York, 2010)
31. F. Rahmani, M. Shahriari, Hybrid photoneutron source optimization for electron accelerator-based BNCT. Nucl. Instrum. Methods Phys. Res. A **618**(1–3), 48–53 (2010)
32. M. Mamtimin, F. Harmon, V. Starovoitova, Electron linac based mixed-field transmutation of 129I. Nucl. Instrum. Methods Phys. Res. B **344**, 11–15 (2015)
33. A. Tsechanski, A. Bielajew, J. Archambault, E. Mainegra-Hing, Electron accelerator-based production of molybdenum-99: bremsstrahlung and photoneutron generation from. Nucl. Instrum. Methods Phys. Res. B **366**, 124–139 (2016)
34. M. Tatari, A.H. Ranjbar, Design of a photoneutron source based on 10 MeV electrons of radiotherapy linac. Ann. Nucl. Energy **63**, 69–74 (2014)
35. M.Y. Satri, et al., Target investigation driven by a 10 MeV electrn linac for bremesstrahlung production, in Proceedings of IPAC2017, Copenhagen, Denmark, ISBN 978-3-95450-182-3 (2017)
36. N.S. Kulkarni et al., Physics design of a 10 MeV, 6 kW travelling wave electron linac for industrial applications. Pramana J. Phys. **87**(5), 20 (2016)
37. T. Kii, et al., Performance of the LaBr3(Ce) scintillator for nuclear resonance fluorescence experiment, in IEEE Nuclear Science Symposium Conference Record (2009), pp. 1490–1492

38. R. Uhlář et al., A new reflector structure for facility thermalizing D-T neutrons. J. Radioanal. Nucl. Chem. **300**(2), 809–818 (2014)
39. R.J. McConn Jr, et al., Compendium of Material Composition Data for Radiation Transport Modeling, PNNL-15870 Rev. 1, Pacific Northwest National Laboratory, 2011
40. https://www.united.com/ual/en/us/fly/travel/baggage/carry-on.html
41. https://www.aa.com/i18n/travel-info/baggage/carry-on-baggage.jsp
42. https://www.lufthansa.com/us/en/carry-on-baggage
43. Iaea, Database of Prompt Gamma Rays from Slow Neutron Capture for Elemental Analysis, Vienna: International Atomic Energy Agency (Iaea) (2007)
44. G.R. Gilmore, *Practical Gamma-ray Spectrometry*, 2nd edn. (Wiley, New York, 2008)
45. M.R. Mohammadian-Behbahani, S. Saramad, A comparison study of the pile-up correction algorithms. Nucl. Instrum. Methods Phys. Res. Sect. A **951**, 72 (2020)
46. XCOM, National Institute of Standards and Technology. http://physics.nist.gov/PhysRefData/Xcom/html/xcom1.html
47. A.N. Dovbnya, et. al, Electron-linac-based radiation facilities of the Ukrainian National Science Center KIPT, in Proceedings of the 1997 Particle Accelerator Conference (Cat. No.97CH36167), IEEE (1997)
48. M.M. Rafiei, H. Tavakoli-Anbaran, Calculation of the exposure buildup factors for x-ray photons with continuous energy spectrum using Monte Carlo code. J. Radiol. Prot. **38**(1), 68 (2018)